

Characterization of Supernovae Based on the Spectral-Temporal Energy Distribution: Possible two SN Ib Subtypes

OFEK BENGYAT^{1,2} AND AVISHAY GAL-YAM¹

¹*Department of Particle Physics and Astrophysics, Weizmann Institute of Science, 76100 Rehovot, Israel*

²*Faculty of Physics, University of Vienna, Boltzmannngasse 5, 1090 Vienna, Austria*

(Received 21 Feb 2022; Revised 24 Mar 2022; Accepted 25 Mar 2022)

Submitted to ApJ

ABSTRACT

A quantitative data-driven comparison among supernovae (SNe) based on their spectral time series combined with multi-band photometry is presented. We use an unsupervised Random Forest algorithm as a metric on a set of 82 well-documented SNe representing all the main spectroscopic types, in order to embed these in an abstract metric space reflecting shared correlations between the objects. We visualize the resulting metric space in 3D, revealing strong agreement with the current spectroscopic classification scheme. The embedding splits Type Ib supernovae into two groups, with one subgroup exhibiting broader, less prominent, higher-velocity lines than the other, possibly suggesting a new SN Ib subclass is required. The method could be to classify newly discovered SNe according to their distance from known event groups, or ultimately to devise a new, spectral-temporal classification scheme. Such an embedding could also depend on hidden parameters which may perhaps be physically interpretable.

1. INTRODUCTION

The existing classification scheme of supernovae (SNe, [Filippenko 1997](#); [Gal-Yam 2017](#)) has been successful in sorting out the majority of objects discovered, in a way that facilitates their study or practical use, e.g. as standard candles ([Riess et al. 1998](#); [Perlmutter et al. 1999](#)). It does that by relying mainly on their spectra.

The current classification scheme divides SNe to Type I and Type II, comprised of SNe lacking H-lines and containing them, respectively. The reason for this is mostly historical ([Minkowski 1941](#)), and modern understanding distinguishes between two other categories based on the progenitor star and the underlying physical explosion process. The first class is thermonuclear SNe, including mostly members of the spectroscopic Type Ia group, that were found ([Nugent et al. 2011](#)) to be a result of a white dwarf (WDs) progenitor, exploding in a manner still actively researched ([Magee et al. 2021](#); [Polin et al. 2019](#)). Spectroscopically, normal Type Ia SNe are identifiable by the strong Si II 6355Å line seen in peak spectra; though this is less clear in some sub-types. The rarer group of Ca-rich Type I SNe has also been associated with long-lived, WD progenitors ([Perets et al. 2010](#); [De et al. 2020](#)). The second category is core-collapse SNe, originating from massive stars whose self-gravity ceases to be supported by nuclear fusion in their core. These are further divided into the H-rich Types II and IIn, the latter distinguished by their narrow Balmer emission lines ascribed to circumstellar material (CSM), and the stripped-envelope SN Types, which are the explosive deaths of massive stars which have already lost their outer hydrogen shell prior to explosion. These include Types Ib and Ic, the latter differing by the lack of He in peak spectra (in particular, the 5876Å, 6678Å, and 7065Å lines). Type IIb SNe exhibit hydrogen lines only in early spectra, which later disappear, indicating a much thinner layer of H in their progenitor star than those of normal Type II SNe. He-poor stripped-envelope SNe with broad spectral lines belong to Type Ic-BL, corresponding to explosions with larger kinetic energy per unit mass, and hence higher ejecta velocity – up to about threefold compared to the $\sim 10^4$ km/s of normal Type Ic SNe. While these are the main, most frequently observed Types, others exist, including stripped-envelope SNe with CSM interaction of Types Ibn (e.g., [Pastorello et al. 2008](#)) and Icn ([Gal-Yam et al. 2021](#)), superluminous SNe (e.g., [Gal-Yam 2019](#)), as well as numerous subdivisions of the Types mentioned here. A recent review about the current classification scheme of SNe could be found in [Gal-Yam \(2017\)](#).

In practice, an experienced individual could examine a spectrum of some SN, mainly by looking at emission or absorption lines, determine its type and enter it to some database. The problem of subjectivity that could possibly emerge in this human classifier scenario has been treated by developing tools such as `Superfit` (Howell et al. 2005) or `SNID` (Blondin & Tonry 2007), both relying on a template bank of SN spectra to which a query spectrum is compared. Considerations such as redshift, reddening through Milky Way or host dust, photometric calibration of the spectrum and contamination by host lines are present in these methods as fit parameters or have their effects diminished by smoothing or continuum estimation and subtraction. These methods, as opposed to human classification, standardize the treatment of different SNe such that different reddening or contamination conditions have less impact on the classification, and they are also more objective, being independent of the user, his attention to details or other forms of human error. The use of such automatic tools also streamlines the task of classification of large amounts of data. Another quantitative approach to classification, of Type I SNe, also relying on peak spectra, was presented by Sun & Gal-Yam (2017). This classification uses the estimation of the depths of a line around 6150Å attributable to Si II or H, depending on the SN, and of O I 7774Å and achieves significant separation between the main Type I SN subtypes (Ia, Ib and Ic), as well as between different Ia subtypes.

However, one drawback in the presently available schemes and methods which still awaits remedy is that they do not rely on the entirety of information available for a SN, but on a single spectrum of it, i.e. from a single epoch. This could also lead to ambiguity, this time not a subjective, user-dependent one, but the mere fact that the current scheme could assign different types to the same object when faced with different spectra of it. An example is Type IIb, which includes core-collapse SNe exhibiting H in early spectra but not in later ones. Prentice & Mazzali (2017) have approached the study of this type-continuum by distinguishing between 4 sub-types ranging from Ib to IIb based on the H α emission and absorption lines. They also treated the continuum between the He-poor stripped core-collapse SNe Types Ic and Ic-BL, the latter being defined by significantly higher explosion velocities than the former, evident in the breadth of spectral lines. This difference in velocities is, just as the Ib–IIb case, not only a continuous parameter discretized into two groups, but also a time-dependent property, as they show that it changes throughout the lifetime of the transient. They do this by examining in practice the related (though only weakly correlated) property of feature count, and divide the continuum into 5 subtypes depending on the average of the feature count over a certain time interval. Examples for He-poor stripped core-collapse events of uncertain classification are SN2004aw (Mazzali et al. 2017) and SN2016coi (Kumar et al. 2018). Additionally, a certain confusion in the classification of stripped core-collapse SNe as Ib or Ic exists. One reason for it is the presence of He, observed in some events initially classified as Type Ic (e.g., SN2007gr, SN2009jf). This has been perceived as a flaw in the current classification scheme, rather than an incomplete physical understanding of the objects (Dessart et al. 2012; Valenti et al. 2011; Blondin & Tonry 2007).

There exists then a certain need for a classification scheme both quantitative and taking into account the entire *spectral-temporal* energy distribution of a SN (i.e., the spectral flux $f(t, \lambda)$ along both wavelength and time) in order to provide a more definite answer about the degree of similarity between, and thus the proper taxonomic sorting of SNe. Such a method could perhaps further unveil some structure in the space of SNe, possibly in the form of a few hidden parameters controlling their properties. Those might, ideally, be later ascribed to physical properties through correlation analysis.

1.1. Machine Learning Methods in Astronomy

Various methods of data analysis have been used in astronomy, the emphasis being put in recent years on machine learning methods. A few examples for uses in the context of SN classification are Sasdelli et al. (2014, 2016); Williamson et al. (2019). Fremling et al. (2021) presents a binary deep-classifier named `SNIScore`, which succeeds in classifying SNe as Type Ia with very low error rates. See also Baron (2019) for a useful review on machine learning methods in astronomy, including those used in this work. The question of quantitative SN classification could be approached by means of some machine learning algorithm which would be trained on feature vectors describing a set of SNe. This training set should then ideally consist of well-sampled SNe, whose classification and comparison to other objects is well-understood. After training, the algorithm should be able to provide new insight about this taxonomy of and similarity between objects when input SNe from or outside of the training set. The method we use in this work is an unsupervised Random Forest (RF) serving as a metric (Shi & Horvath 2006), which has been found viable in defining a distance between spectra (Baron & Poznanski 2016; Reis et al. 2018). Section 3.3 describes the algorithm and its application.

2. OBJECTIVE

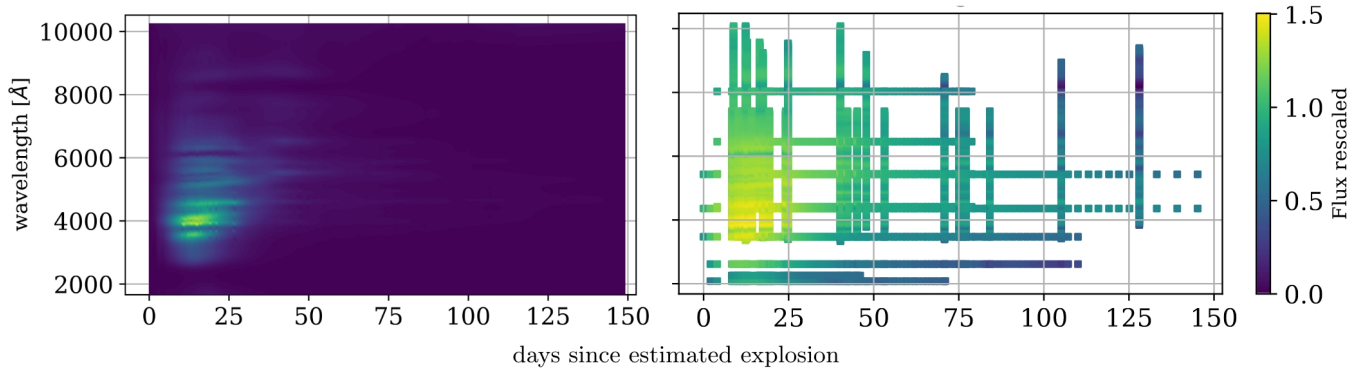


Figure 1. An example of the output (left) and input (right) of PyCoCo for SN2007af. The interpolated, calibrated and dereddened rest-frame flux function $f(t, \lambda)$ can be seen on the left, and the input spectral and photometric data is on the right. Note that the colors on the right panel differ from those on the left as the input spectra and photometry are not yet calibrated or dereddened.

In this work, we present a method to characterize, or classify, SNe based on their spectral-temporal energy distribution by means of a data-driven embedding in an abstract metric space. We compare the spectroscopic types in the current scheme – as determined by a human expert after examining the spectral sequence available for the SN in question – with the resulting embedding.

Other than this comparison, we examine possible Type-continua or new subtypes which may arise from the embedding.

3. METHOD

3.1. Estimating the Spectral-Temporal Energy Distribution of a SN

The raw data of each SN, i.e. its spectra and multi-band photometry, are processed with PyCoCo, a program for template creation of spectral energy distribution of SNe developed by Vincenzi et al. (2019, hereafter V19). It uses Gaussian Process Regression to interpolate the flux in the intervals between the input spectra, with the photometry data used both for flux calibration of the spectra and as data points. PyCoCo also corrects the flux for Milky Way extinction and host extinction¹ values the user inputs, and removes tellurics and host lines, as well as transforming the data into the rest frame of the SN. The final output from PyCoCo is the (normalized) rest-frame spectral energy distribution $f(t, \lambda)$ of the input SN on some grid of time and wavelength.

We keep the power n of the light-curve rising fit in PyCoCo, $f \propto (t - t_0)^n$, (V19, Eq. 2) as a free parameter for all the SNe we apply it on, and we also choose to not extend and oversample the light-curves at late times, as our analysis concentrates on relatively early times (see next section). As the majority of PyCoCo outputs used in this work were generated by V19 (see Section 4), it should be mentioned that they only left n as a free parameter in cases where the photometric data shortly after explosion was good enough to allow a reasonable fit. When not, n was fixed to a value, which depends on whether the SN is H-rich (Types II and II_n) or not (the rest of the types), as indicated by the user. This is the only place where input regarding classification is used in PyCoCo. It should also be noted that a different light curve rise model was used for the data sets of Type II_b SN1993J, SN2011dh, SN2011fu, and SN2013df generated by V19, in order to take into account their double early peaks. This is also true for SN2006aj, but in this case its double peak is likely a result of its unusually early detection, rather than an actual peculiarity (Mirabal et al. 2006), so we omit the first peak data for this object. Readers are referred to Section 2.1 in V19 for details about the light-curve fits in PyCoCo.

The code used in this section is available on GitHub². See Figure 1 for an example of the process.

3.2. Preparation of Feature Vectors

¹ Host uncorrected output is also produced, though in this work we only use the host corrected versions.

² https://github.com/ofek-b/PyCoCo_templates

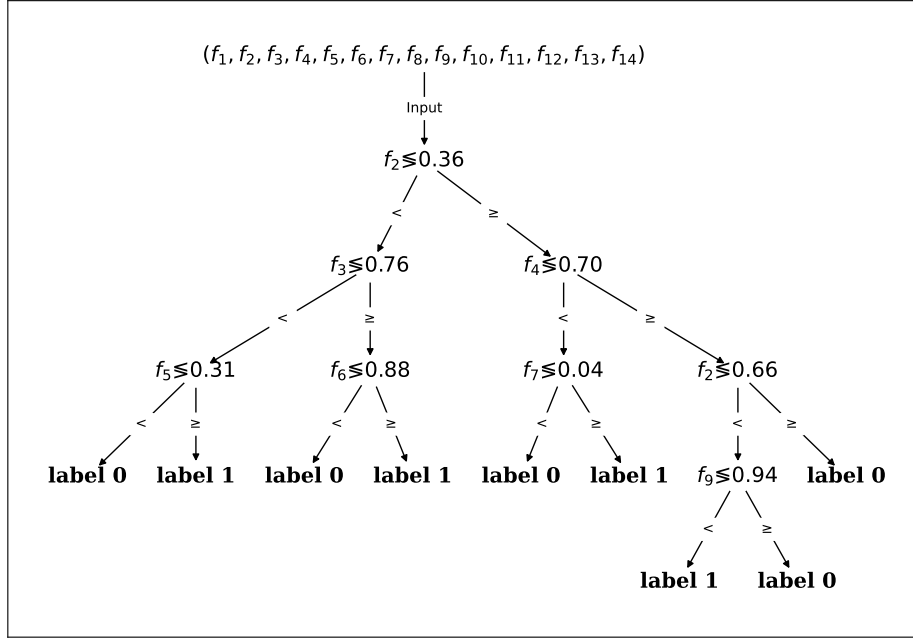


Figure 2. An illustration of a trained binary Decision Tree, multiple different instances of which comprise an RF. The input object propagates according to its features f_i .

We use an algorithm from Carnall (2017)³ to rebin in wavelength and perform linear interpolation in time to obtain the fluxes on a uniform grid $T \times \Lambda$ over all SNe, where

$$T = 0 \text{ d to } 50 \text{ d at } 1 \text{ d intervals}$$

$$\Lambda = 4000 \text{ \AA to } 8000 \text{ \AA at } 40 \text{ \AA intervals.}$$

Times are counted since the estimated explosion of each template. We choose this wavelength interval Λ as it is covered available photometric data for almost all SNe in our data set, making the output of PyCoCo more credible. The time interval T is chosen so it includes times where most SNe are not too faint.

As others have done (e.g., Sasdelli et al. 2014, or less directly in Blondin & Tonry 2007), we use the wavelength derivative of the logarithm of the flux of every SN,

$$\tilde{f}(t, \lambda) \equiv \frac{d}{d\lambda} \log f(t, \lambda),$$

instead of the flux itself, in order to emphasize spectral lines and diminish the effect of the unaccounted for reddening. The data is then sorted in an N -row matrix X , where each row X_i corresponds to the i -th SN in our data set:

$$X_i = (\tilde{f}(t_j, \lambda_j))_{(t_j, \lambda_j) \in T \times \Lambda}.$$

In order to account for some missing data points we then use the Expectation Maximization Principle Component Analysis (EMPCA) algorithm presented in Bailey (2012)⁴ on our feature matrix X to produce a principal components matrix, P_C , which is then immediately transformed back to the feature space to produce X_C , now without missing data. The number of principal components we choose is $C = 50$, which preserves 93% of the variance.

3.3. Unsupervised Random Forest as a Metric

We now train an unsupervised RF on the data in X_C and use it as a metric on the set of SNe as described by the same matrix X_C . This section describes this process.

³ <https://github.com/ACCarnall/spectres>

⁴ <https://github.com/sbailey/empca>

RF is originally a supervised machine learning classifier (Ho 1995). A brief description of it follows, regarding only binary classification as relevant for this work. First, we describe binary Decision Trees. A Decision Tree is a supervised classifier by itself, structured as a tree graph – a directed graph with a single start node, several terminal nodes and several ”generations” of intermediate nodes in between, where every intermediate node has exactly one arrow pointing to it from its parent and exactly two arrows which it points to its children. When an object is queried into the Decision Tree, each non-terminal node k hands it over to one of its two child nodes, chosen according to the truth value of a condition of the form $f_{i_k} < c_k$, where f_{i_k} is the value of the i_k -th feature of the Tree input, and c_k is a real number. The training process consists of the simultaneous input of all objects in the training set. Before propagating a set of objects which has arrived to any node k , the training algorithm chooses the parameters i_k and c_k providing the best separation between the known labels for the objects. The definition of goodness of separation is a matter of choice (a so-called hyperparameter). When all of the objects which arrived in a node are of the same label, this node is set as a terminal node and is assigned the label. Training ceases when all objects arrived at terminal nodes. Classifying a queried object occurs by propagating it through the trained Decision Tree and returning the label corresponding to the terminal node it reaches. Note that Decision Trees and their training process are deterministic. See Figure 2 for an illustration and the classification scheme for Type I SNe presented in Sun & Gal-Yam (2017, Section 4.2) for a working example.

An RF consists of multiple Decision Trees. Every Tree is (i) only trained on a random subset of the training set, and (ii) only allowed to use a random subset of the features. The class assigned to a queried object is determined by a majority vote of all the Decision Trees in the Forest. An RF is thus an ensemble learning method, aggregating the results of the Trees to achieve better accuracy and robustness. In order to use an RF as a metric, one performs the following *unsupervised* training process. The training data set in question is used to create a synthetic data set of the same size. The samples in the synthetic data set have the same number of features as in the original data set and the same marginal distributions for each feature, but zero correlations between features. Supervised training follows, as described above, using the real and synthetic sets, where the real set is assigned the label **real** and the synthetic set is assigned the label **synth**. Note that these labels have nothing to do with SN types or with the data itself in any way, and they merely differentiate between the real, correlation exhibiting data, and the synthetic, uncorrelated data. After training, the similarity returned for two queried objects is the fraction of Trees in the Forest for which the two objects end up in the same terminal node, out of only the Trees which assign label **real** for both objects (i.e., the correct label, as one tries to find the similarity measure between two real objects). The metric, distance or dissimilarity (used interchangeably in this work) is obtained by subtracting the similarity from unity.

This similarity measure thus learns the most prominent correlations in the training data, and measures to which extent do two given objects share such correlations. One such correlation could be, for instance, the presence of all three strongest He lines in a spectrum, as opposed to only some of them.

The algorithm we use was written by Baron & Poznanski (2016)⁵. The number of Trees used is 2000, and the separability criterion is the Gini Impurity. The output of our analysis is the distance matrix for our SN data set, with entries between 0 and 1.

The code used in Sections 3.2 and 3.3, as well as in the following visualization of the results is available on GitHub⁶.

4. DATA

Alongside the description of the PyCoCo code, V19 also includes the code output for 67 core-collapse SNe, listed in Table 2 of their publication. Our data set is built upon those SNe, with some exclusions and type changes of SNe listed in Table 1. We extend this data set by adding the SNe listed in Table 2. The final list of 82 SNe used in this work is given in Table 3, along with the Data Quality Index (DQI) described next. This data set will be made available upon request.

Two SN Types missing from the V19 set, which we also did not add, are Ca-rich SNe and H-poor superluminous SNe (SLSN-I). In the case of Ca-rich SNe, the reason is the poor data sets available for those objects. In the case of SLSN-I, peak light often occurs late, and outside our temporal window, such that our selected time grid would miss important information about those objects, the same holds also for SN1987A-like Type II SNe. One could envision including these groups once more data are available, and including a temporal renormalization for SLSNe-I and 87A-like events.

⁵ <https://github.com/dalya/WeirdestGalaxies>

⁶ https://github.com/ofek-b/spectra_in_time

Table 1. The SNe from V19 which were excluded from the training set in this work or whose assigned spectroscopic type was changed after examining their spectral series.

Name	Type in V19	Comments
<i>Excluded:</i>		
SN1987A	87A-like	long rise time with peak outside our temporal range
SN2005bf	Ib	very anomalous, double-peaked light curve (Folatelli et al. 2006)
SN2008D	Ib	highly extinguished (Rabinak & Waxman 2011); unique early time data
SN2011bm	Ic	very wide light curve (Valenti et al. 2012)
SN2016bkv	II	faint, unusually long light curve, weaker lines (Nakaoka et al. 2018)
SN2008in	II	DQI < 0.8
SN2009dd	II	DQI < 0.8
SN2013fs	II	added again manually for the analysis in Section 5.3. appears on Table 2.
SN2008aq	I Ib	DQI < 0.8
SN2009ip	II In	peculiar object, may not be a SN (Mauerhan et al. 2013)
SN2011ht	II In	DQI < 0.8
<i>Type changed:</i>		
SN2009jf	Ib	changed to Ic, see Gal-Yam (2017)
SN2010al	II In	changed to Ib In (Pastorello et al. 2015)
SN2008fq	II In	changed to II
SN2007pk	II In	changed to II

For the SNe we added, spectra were taken from WISeREP⁷ (Yaron & Gal-Yam 2012) and photometry from the Open Supernova Catalog⁸ (Guillochon et al. 2017), where available. The values for Milky Way reddening $E(B - V)_{\text{MW}}$ were taken from Schlafly & Finkbeiner (2011). The host reddening estimations $E(B - V)_{\text{host}}$ were taken from the provided references. When no estimation could be found, the median value for the SN type was taken.

4.1. Data Quality Index

The quality of the output of PyCoCo depends on the coverage of the spectral-temporal region $T \times \Lambda$ by the spectroscopic and photometric data of each object. A Data Quality Index (DQI) between 0 and 1 is thus calculated for each SN in the following manner. For each point on the $T \times \Lambda$ grid, the distance to the nearest input data point (spectroscopic or photometric) is calculated as the usual Euclidean distance, where the time and wavelength axes are normalized by their total length. The fraction of grid points which are closer than 0.1 to a data point is defined as the DQI. We only included SNe with $\text{DQI} \geq 0.8$ in our analysis. The impact of this choice is minimal (the removal of 4 objects; Table 1).

5. RESULTS

After applying the EMPCA algorithm, the fraction of data variance explained is 93%. Figure 3 shows the distance matrix D resulting from an unsupervised RF as described. It is not completely symmetrical due to computation errors – the median absolute symmetric difference of off-diagonal terms is 0.005 – so we enforce symmetry by using $\frac{1}{2}(D + D^T)$ as the dissimilarity matrix. A certain degree of block-diagonality is noticeable, expressing agreement with the current classification scheme for these well-documented SNe.

5.1. Visualization of The Metric Space

For visualisation of this dissimilarity matrix inside a low-dimensional Euclidean space while trying to preserve structure, we use t-Distributed Stochastic Neighbor Embedding (tSNE), developed by van der Maaten & Hinton (2008). The visualization in 3d space is shown in Figure 4, with colors representing the spectroscopic type assigned by a human expert after manually inspecting the evolution of spectra available for the SN. Examining the visualization one can notice the aforementioned block-diagonality in the form of well-separated clusters which are relatively homogeneous

⁷ <https://wiserep.weizmann.ac.il>

⁸ <https://sne.space>

Table 2. The SNe used for training in this work in addition to those from V19.

Name	z	Type	Photometry	# Spec.	$E(B - V)_{\text{host}}$	Ref.
SN2013fs	0.011855	II	$UVW2, UVM2, UVW1, U, B, V, R, I$	23	0.015	(1-3)
SN2017gpn	0.007388	Ilb	B, V, g, r, i	8	0.000	(4)
SN2006el	0.017000	Ilb	B, V, R, r, i	6	0.081	(5-9)
SN1996cb	0.002372	Ilb	B, V, R	8	0.120	(5, 7, 10-11)
SN2015ap	0.011400	Ilb	B, V, u, g, r, i	17	0.000	(4-5)
SN2010jl	0.010700	IIIn	$UVW2, UVM2, UVW1, U, B, V, u, r, i$	3	0.022	(12-16)
SN2011fe	0.000804	Ia	$UVW2, UVM2, UVW1, U, B, V, R, I, r$	27	0.014	(13, 17-28)
SN2012fr	0.004000	Ia	$UVW2, UVM2, UVW1, U, B, V, R, I, g, r, i$	22	0.000	(13, 22, 24, 29-31)
SN2017erp	0.006174	Ia	$UVW2, UVM2, UVW1, U, B, V, R, I$	11	0.097	(13, 20, 22, 26, 32)
SN2005cf	0.006461	Ia	$UVW2, UVM2, UVW1, U, B, V, R, I$	23	0.100	(13, 26, 33-36)
SN2012ht	0.004000	Ia	$UVW2, UVM2, UVW1, U, B, V, R, I, g, r, i$	14	0.000	(13, 22, 37-39)
SN2011by	0.002843	Ia	$UVW2, UVM2, UVW1, U, B, V, R, I$	11	0.039	(13, 17, 20, 26, 40-41)
SN2009ig	0.008770	Ia	$UVW2, UVM2, UVW1, U, B, V, R, I$	12	0.000	(13, 17, 20, 22, 26, 42-43)
SN2007af	0.005464	Ia	$UVW2, UVM2, UVW1, U, B, V, R, I$	14	0.130	(13, 26, 34, 44-47)
SN2004dk	0.005200	Ib	B, V, R, I	8	0.180	(7-8, 48-50)
SN2015ah	0.016000	Ib	B, V, u, g, r, i, z	9	0.020	(4-5)
SN2016jdw	0.018900	Ib	u, g, r, i, z, c, o	5	0.000	(4)
SN2017bgu	0.008000	Ib	u, g, r, i, z, c, o	7	0.020	(4)
SN1999ex	0.011414	Ibc	U, B, V, R, I	5	0.028	(51-52)
SN2006lc	0.016200	Ibc	B, V, g, r, i, z	6	0.298	(5-7, 13, 53-56)
SN2019deh	0.054690	Ibn	g, r, i, z	9	0.224	(9, 57)
SN2019aaajs	0.035800	Ibn	g, r, i, z	4	0.224	(9, 57)
SN2019iep	0.057000	Ibn	g, r	7	0.224	(9, 57)
SN2014L	0.008029	Ic	U, B, V, R, I	13	0.630	(5, 58)
SN2016coi	0.003600	Ic-BL	$UVW2, UVM2, UVW1, U, B, V, R, I, g, r, i$	48	0.000	(13, 59-61)
SN2003jd	0.018860	Ic-BL	B, V, R, I	10	0.100	(5-7, 62)

References—(1) Valenti et al. (2016); (2) Yaron et al. (2017); (3) Childress et al. (2016); (4) Prentice et al. (2019); (5) Shivvers et al. (2019); (6) Bianco et al. (2014); (7) Modjaz et al. (2014); (8) Drout et al. (2011); (9) median $E(B - V)_{\text{host}}$ value, Prentice et al. (2016); (10) Qiu et al. (1999); (11) Matheson et al. (2001); (12) Zhang et al. (2012); (13) Brown et al. (2014); (14) Jencson et al. (2016); (15) Fransson et al. (2014); (16) Smith et al. (2012); (17) Smitka et al. (2016); (18) Pereira et al. (2013); (19) Zhang et al. (2016); (20) Stahl et al. (2019); (21) Munari et al. (2013); (22) Stahl et al. (2020); (23) Parrent et al. (2012); (24) Graham et al. (2017); (25) Mazzali et al. (2014); (26) Silverman et al. (2012); (27) Nugent et al. (2011); (28) Firth et al. (2015); (29) Childress et al. (2013); (30) Contreras et al. (2018); (31) Zhang et al. (2014); (32) Brown et al. (2019); (33) Wang et al. (2009); (34) Ganeshalingam et al. (2010); (35) Garavini et al. (2007); (36) Pastorello et al. (2007); (37) Vinkó et al. (2018); (38) Yamanaka et al. (2014); (39) Burns et al. (2018); (40) Silverman et al. (2013); (41) Foley et al. (2020); (42) Foley et al. (2012); (43) Brown et al. (2012); (44) Simon et al. (2007); (45) Sternberg et al. (2011); (46) Brown et al. (2010); (47) Blondin et al. (2012); (48) Shivvers et al. (2017); (49) Modjaz et al. (2008); (50) Harutyunyan et al. (2008); (51) Hamuy et al. (2002); (52) Stritzinger et al. (2002); (53) Stritzinger et al. (2018); (54) Ostman et al. (2011); (55) Sako et al. (2018); (56) Stritzinger et al. (2018); (57) Kool et al. in preparation; (58) Zhang et al. (2018); (59) Terreran et al. (2019); (60) Prentice et al. (2018); (61) Kumar et al. (2018); (62) Valenti et al. (2008)

in type. We remind the reader that the spectroscopic types represented by the colors were not used in the analysis which led to the dissimilarity matrix or the visualization (the only exception is mentioned in Section 3.1).

Another way to visualize the results is to look at the Minimum Spanning Tree (MST) of the fully-connected graph defined by the distance matrix. The MST is a fully-connected subgraph minimal in the sum of edge weights⁹ (here – distances) and is shown in Figure 5. The algorithm by Yamada et al. (2010)¹⁰ was used. The concept of MST in

⁹ The MST is generally not unique, though it is unique in this case.

¹⁰ <https://github.com/dakota-hawkins/yamada>

Table 3. All SNe used for training in this work and the DQI calculated for them.

Type	Names (DQI)
II	ASASSN14jb (0.91), ASASSN15oz (0.89), SN1999em (0.98), SN2004et (0.83), SN2005cs (0.96), SN2007od (0.91), SN2007pk (0.92), SN2008bj (0.83), SN2008fq (0.95), SN2009N (0.84), SN2009bw (0.83), SN2009ib (0.87), SN2009kr (0.90), SN2012A (0.97), SN2012aw (1.00), SN2013ab (0.99), SN2013am (0.97), SN2013by (0.95), SN2013ej (1.00), SN2013fs (1.00), SN2014G (1.00), SN2016X (1.00)
I Ib	SN1993J (1.00), SN1996cb (0.87), SN2006T (0.95), SN2006el (0.84), SN2008ax (1.00), SN2008bo (0.91), SN2011dh (1.00), SN2011ei (0.95), SN2011fu (1.00), SN2011hs (0.96), SN2013df (0.85), SN2015ap (0.99), SN2016gkg (0.95), SN2017gpn (0.97)
I In	SN2006aa (0.92), SN2010jl (0.90)
Ia	SN2005cf (1.00), SN2007af (0.93), SN2009ig (0.91), SN2011by (0.99), SN2011fe (0.99), SN2012fr (1.00), SN2012ht (0.99), SN2017erp (0.99)
Ib	SN1999dn (0.90), SN2004dk (0.87), SN2004gq (0.92), SN2004gv (0.90), SN2005hg (0.95), SN2006ep (0.86), SN2007Y (0.96), SN2007uy (0.83), SN2009iz (0.91), SN2015ah (0.92), SN2016jdw (0.90), SN2017bgu (0.86), iPTF13bvn (1.00)
Ibc	SN1999ex (0.91), SN2004gt (0.80), SN2006lc (0.87), SN2012au (0.81)
Ibn	SN2010al (0.94), SN2019aajs (0.88), SN2019deh (0.98), SN2019iep (0.97)
Ic	SN1994I (0.96), SN2004aw (0.85), SN2004fe (0.96), SN2007gr (0.96), SN2009jf (0.94), SN2013ge (0.99), SN2014L (0.94)
Ic-BL	SN1998bw (0.89), SN2002ap (0.99), SN2003jd (0.89), SN2006aj (0.93), SN2007ru (0.88), SN2009bb (0.92), SN2012ap (0.91), SN2016coi (0.99)

the context of an abstract dissimilarity space could be employed, as was done by [Baron & Ménard \(2020\)](#), to extract sequences from the data, which could later be compared with physical parameters.

Looking at [Figure 4](#), we see several remarkable features. Objects of Type Ibn are close to those of Type IIn probably due to sharing narrow features. In contrast, the proximity of Type Ic-BL objects to the Type II cluster is unexpected. A possible explanation could be that the features those two groups share with one another are the dominance of the continuum.

One notices the very close pair of objects SN2015ap (I Ib, purple) and SN2004gq (Ib, blue). A possible explanation is that SN2015ap, although exhibiting H-absorption initially, loses them at a relatively early stage, ~ 10 days after explosion, leaving no H evident in its spectrum. Another object to be noticed is SN2004gt (Ibc, cyan) in between the main Ib and Ic clusters, which fits previous classification ([Eldridge et al. 2013](#)). As for SN2007Y (main Ib cluster, blue), its initial classification was Ib despite $H\alpha$ absorption lines observed at early times and it has been claimed that I Ib would be a better classification ([Maurer et al. 2010](#); [Stritzinger et al. 2009](#); [Chevalier & Soderberg 2010](#)). The embedding suggests that it is part of the main Ib cluster, though it is on its edge.

As could also be observed in the tSNE visualization, the Type Ic SN2009jf and SN2007gr (two dark green points in the upper main Ic cluster) are very close by, which fits the fact that they are almost identical spectroscopically in the optical and IR wavelengths throughout their evolution ([Valenti et al. 2011](#)). They are also close to the Ib cluster, with the He-poor SN2007gr slightly differing from SN2009jf which shows stronger He lines, leading [Valenti et al. \(2011\)](#) to classify as Ib, though they acknowledge the possibility that a Ic could be a better choice. Likewise, [Dessart et al. \(2012\)](#) have found that the data of SN2007gr, classified there as Type Ic, may be well explained by a He-rich model, but with weak lines. These authors conclude from their analysis of Type Ib and Ic SNe that the property usually assumed to define Type Ic event, the lack of He, is justified for very few, if any, objects. Indeed, a continuum such as the one visualized in [Figure 4](#), may be a more suitable way to understand those objects.

5.2. The Split of Type Ib SNe

It can be noticed in the visualizations that some Type Ib SNe are set apart from the main cluster formed by this type. The SNe in the main cluster are SN2004gv, SN2007Y, SN2006ep, SN2015ah, SN1999dn, iPTF13bvn, SN2005hg and SN2009iz. The offset Type Ib SNe are SN2004gq, SN2007uy, SN2016jdw, SN2017bgu, SN2004dk and SN2015ap, which is of Type I Ib but still included in this list (see [Section 5.1](#)). [Figure 6](#) shows a comparison between the mean spectra of these two groups.

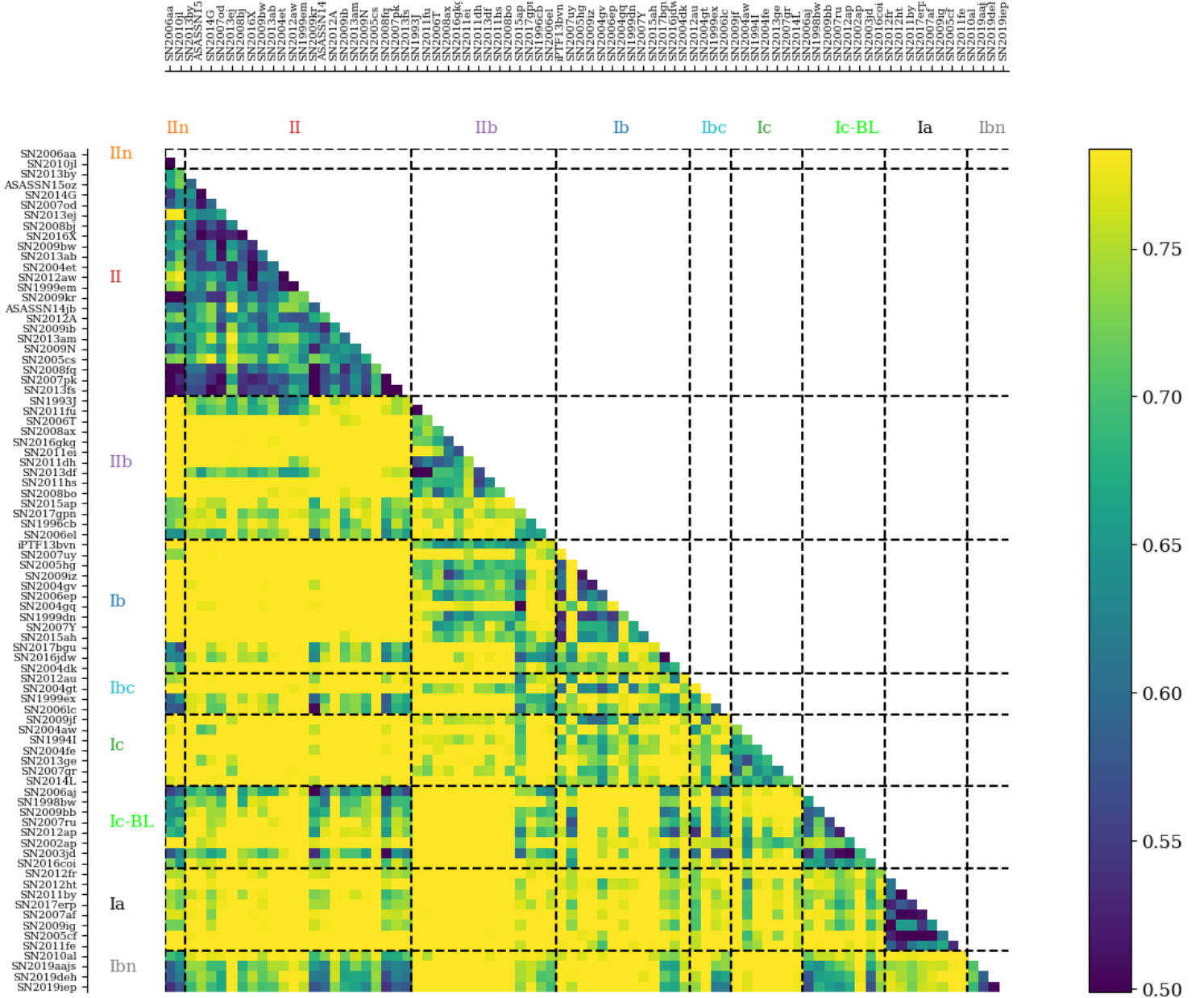


Figure 3. The resulting dissimilarity matrix after applying the RF dissimilarity measure on the data set. Colors represent dissimilarity, are in linear scale and only vary between the 1st and 50th percentile.

The figure suggests that this split could be correlated with the SN expansion velocity, as the features in the mean spectrum of the offset cluster are wider and bluer, especially before- and at peak. To validate this effect, we examine the raw spectra of each event near peak (i.e., prior to any processing of the data). We find that the average expansion velocities derived from the location of the absorption minimum of the He I lines at $\lambda\lambda 5876, 6678, 7065\text{\AA}$ are 9700 ± 1000 and $12300 \pm 1200 \text{ km s}^{-1}$ for the main and offset clusters respectively. The velocities were measured using the dedicated tool on WISeREP. This supports the results of our analysis, and suggests that there may be a split between populations of low-velocity and high-velocity SNe Ib. This of course brings to mind the well-known separation between spectroscopically normal SNe Ic and broad-line, high-velocity SNe Ic-BL (e.g., Modjaz et al. 2016, Gal-Yam 2017, Prentice & Mazzali 2017), though for SNe Ib the velocity spread between normal and high-velocity events may be less extreme, making this division less obvious.

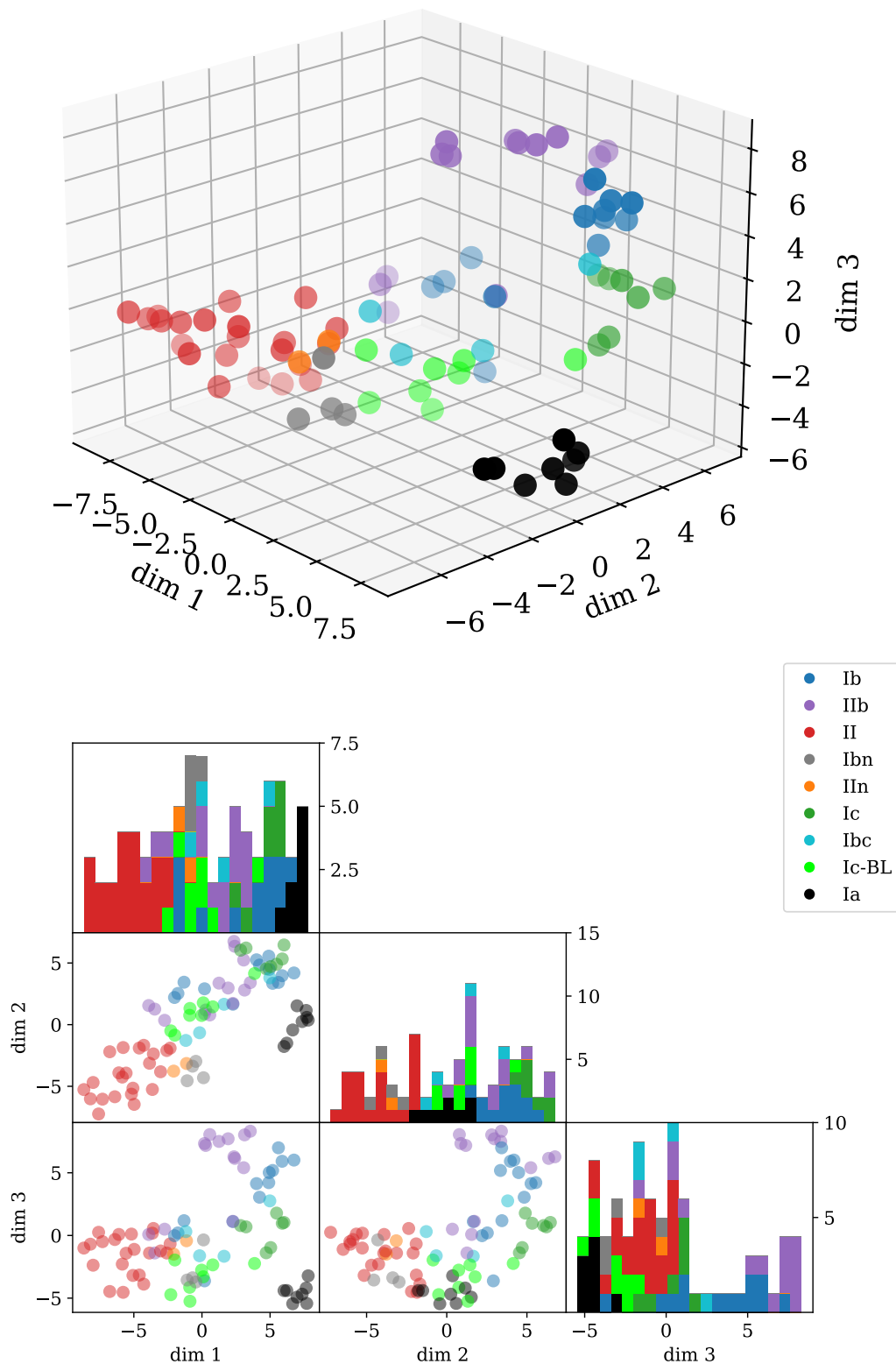


Figure 4. Embedding of the dissimilarity matrix in Figure 3 by tSNE with parameters `perplexity = 10`, `learning_rate = 10`, shown in 3D (top) and in a corner plot (bottom). The KL divergence with respect to the dissimilarity matrix is 0.20. The colors represent the types as assigned for the spectral series by a human expert. The axes represent the coordinates of the embedded Euclidean space. A rotatable version of the top panel is available in the online version and under https://github.com/ofek-b/spectra_in_time/blob/rf_dlog_no_pca/3d_paper.html. The rotation is about the dim 3 axis. The speed and direction of the rotation can be controlled by the buttons or by dragging the slider.

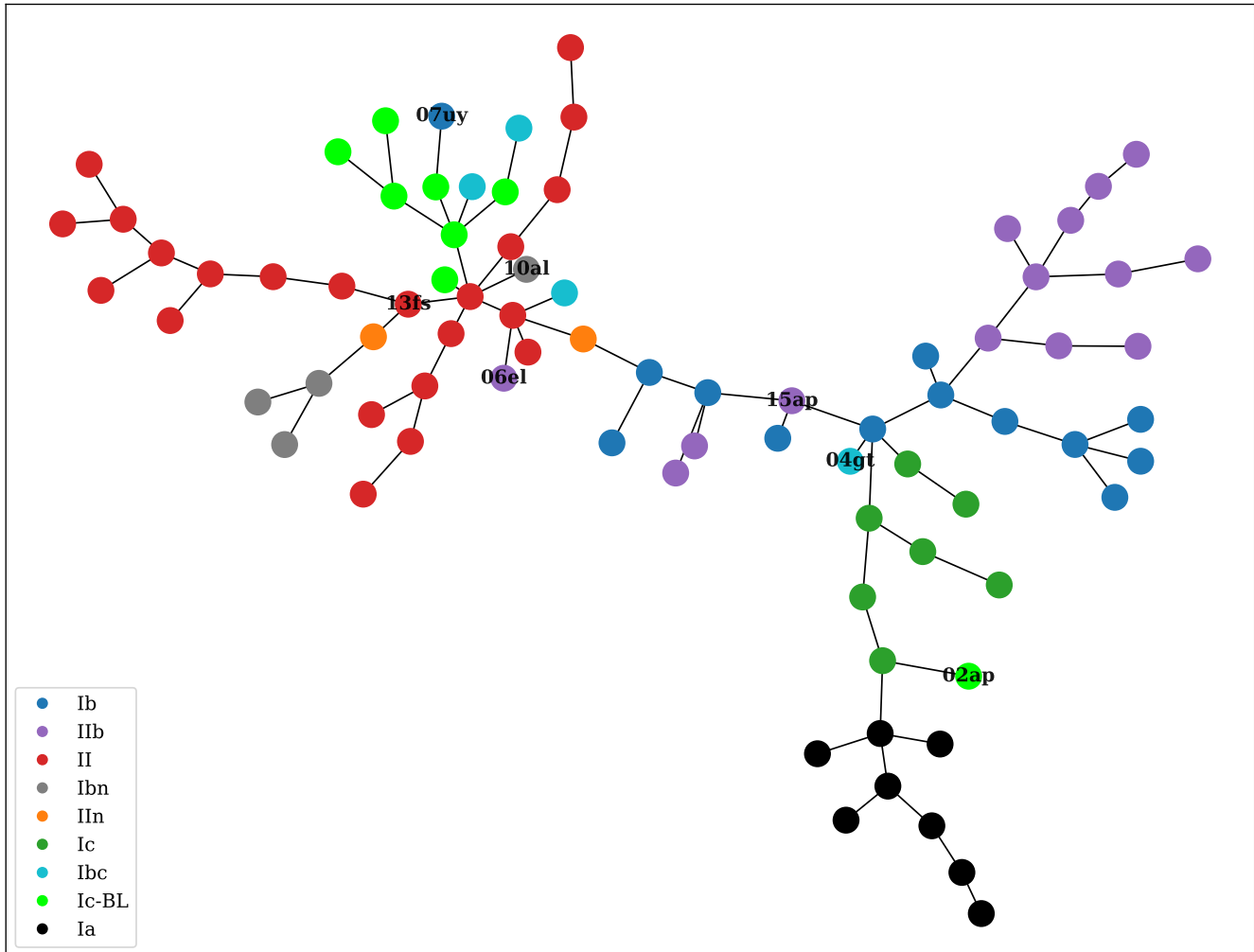


Figure 5. The MST of the graph of SNe defined by the dissimilarity matrix. Note that edge lengths are arbitrary.

5.3. An Application to SNe With Less Data

While the SNe used for training are some of the best observed objects of their types, we wish to test to which extent is the embedding of a new SN with lower amount of data useful. Figure 7 shows the effect of only including two spectra in the input to PyCoCo on the displacement of the embedding relative to the "true" one produced by using all of the data for the SN. We test this on the Type Ia SN2005cf and the Type II SN2013fs. We do not degrade the photometric data in this test. It can be seen that at least for those SNe, using only two spectra does not affect much the quality of embedding. This is highly relevant since future data sets from ongoing and future surveys such as the Zwicky Transient Facility (ZTF; Bellm et al. 2019; Graham et al. 2019) and in the future the Rubin Observatory include high-quality multicolor light curves. Spectroscopy is often obtained as soon as possible after discovery (e.g., Gal-Yam et al. 2011) and again around peak, so a typical future data set may likely include this combination of two spectra and good light curves.

6. CONCLUSION

We present a method for quantitative comparison of SNe by means of an unsupervised embedding in a metric space. This data-driven method identifies the important correlations/spectral features evident in the spectral-temporal energy distributions it is trained on. Other methods which have been used for quantitative classification of SNe (e.g., Sun & Gal-Yam 2017; Prentice & Mazzali 2017) can be understood as supervised decision trees constructed by experienced astrophysicists rather than by an automated training process. Our approach is in principal similar, but chooses an

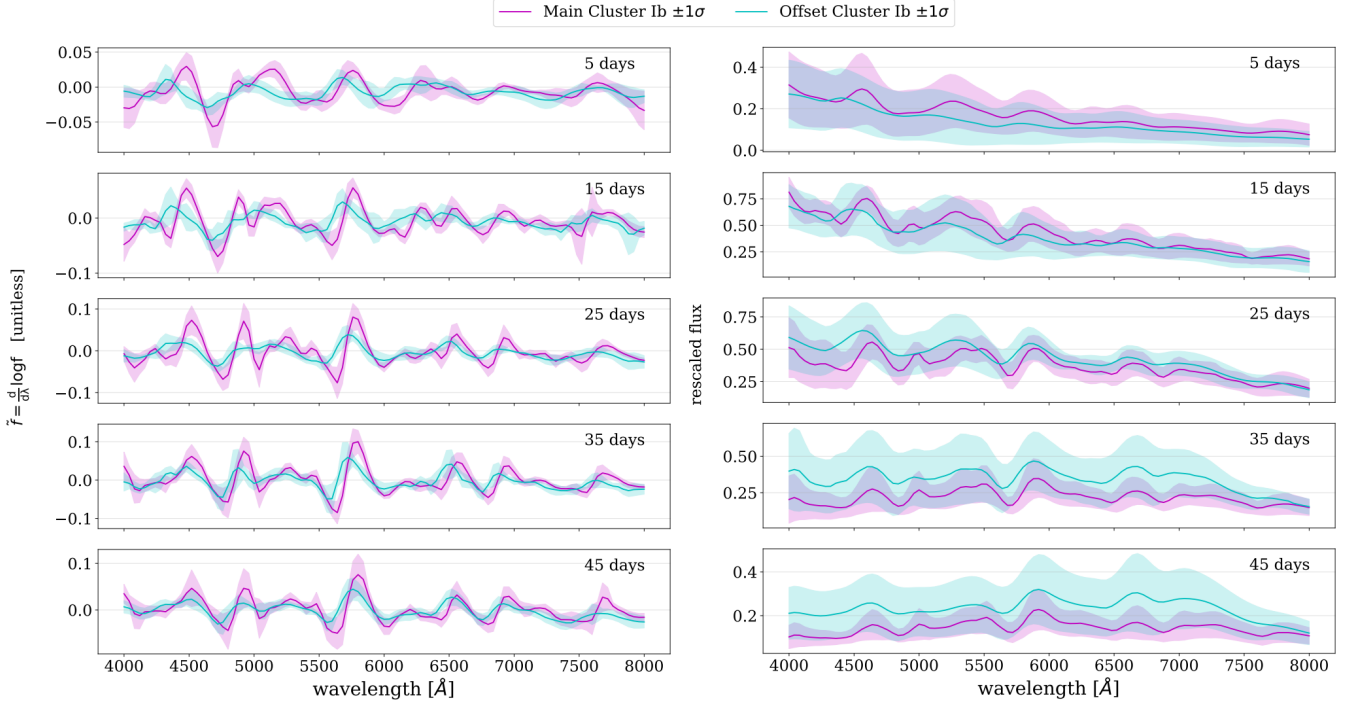


Figure 6. Comparison between the mean spectra as a function of time from explosion of Type Ib SNe from the main cluster and of the rest of the events (see text) in the offset sub-cluster. The flux f (right panel) and its derivative \dot{f} (left panel) are used for the comparison. One can notice (more clearly on the left hand side) that the spectral features are narrower, more prominent and have lower expansion velocity, especially before and at peak, for SNe that belong to the main cluster than for those from the offset one.

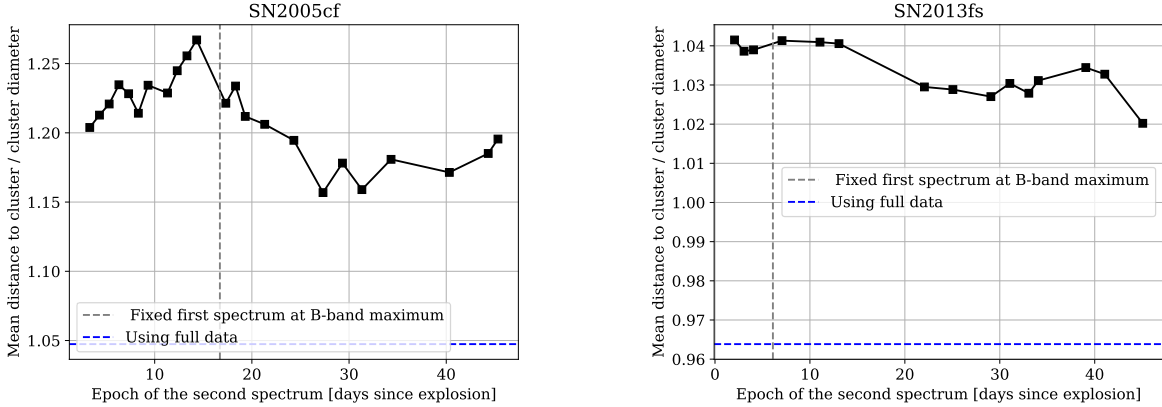


Figure 7. Embedding SN2005cf (Type Ia) and SN2013fs (Type II) with degraded data in a metric space trained on a set not containing these SNe. After training, each SN was embedded in the space using only a subset of the data. The degraded subsets are the PyCoCo output for the entire photometric data, but only two spectra: one at the B-band maximum and the other at the time given on the x-axis. The y-axis is the distance of the embedded degraded form from the respective cluster (Type Ia or Type II SNe), in units of the specific cluster diameter. One can see that the degraded data sets remain in the close vicinity of the mother cluster.

unsupervised method in order to detect the most important correlations – deemed as such by an objective measure – in a given training set. The method succeeds in defining some clusters, which mostly agree with the known spectroscopic Types, and in visualizing the I Ib-Ic-IC-BL continuum. There, objects like SN2007Y, SN2009jf and SN2015ap could

get a quantitative answer regarding their Type by this method, while the classical element-based classification is not as conclusive.

One result our method produces is the possible split of Type Ib SNe into two subgroups, of normal and higher-velocity events, perhaps mimicking the more prominent division between spectroscopically normal SNe Ic and SNe Ic-BL. As discussed earlier, this separation could be of a discrete nature and should be investigated further (preferably with a larger sample) to further validate or dismiss its existence and test the underlying differences in the physics of the explosions.

Preliminary tests show that even a small number of spectra, when combined with multi-band photometric measurements, suffice for obtaining a relatively accurate embedding. This could make the method useful in the context of surveys such as those to be conducted by the Rubin Observatory.

The application as a classifier for less typical SNe should be approached with caution, as the training set needs to contain a wide enough selection of SNe (which in turn need to have enough data) in order to be able to produce a meaningful result.

ACKNOWLEDGMENTS

We thank Dalya Baron, Ido Irani, Barak Zackay and the ZTF collaboration for useful advice, and an anonymous referee for a helpful review.

Software: This work made use of the Python packages NumPy (Harris et al. 2020), Matplotlib (Hunter 2007), scikit-learn (Pedregosa et al. 2011), pandas (Wes McKinney 2010) and NetworkX (Hagberg et al. 2008).

REFERENCES

- Bailey, S. 2012, Publications of the Astronomical Society of the Pacific, 124, 1015–1023, doi: [10.1086/668105](https://doi.org/10.1086/668105)
- Baron, D. 2019, Machine Learning in Astronomy: a practical overview. <https://arxiv.org/abs/1904.07248>
- Baron, D., & Ménard, B. 2020, Extracting the main trend in a dataset: the Sequencer algorithm. <https://arxiv.org/abs/2006.13948>
- Baron, D., & Poznanski, D. 2016, Monthly Notices of the Royal Astronomical Society, 465, 4530, doi: [10.1093/mnras/stw3021](https://doi.org/10.1093/mnras/stw3021)
- Bellm, E. C., Kulkarni, S. R., Graham, M. J., et al. 2019, PASP, 131, 018002, doi: [10.1088/1538-3873/aaecbe](https://doi.org/10.1088/1538-3873/aaecbe)
- Bianco, F. B., Modjaz, M., Hicken, M., et al. 2014, Astrophys. J. Suppl., 213, 19, doi: [10.1088/0067-0049/213/2/19](https://doi.org/10.1088/0067-0049/213/2/19)
- Blondin, S., & Tonry, J. L. 2007, The Astrophysical Journal, 666, 1024–1047, doi: [10.1086/520494](https://doi.org/10.1086/520494)
- Blondin, S., et al. 2012, Astron. J., 143, 126, doi: [10.1088/0004-6256/143/5/126](https://doi.org/10.1088/0004-6256/143/5/126)
- Brown, P. J., Breeveld, A. A., Holland, S., Kuin, P., & Pritchard, T. 2014, Astrophys. Space Sci., 354, 89, doi: [10.1007/s10509-014-2059-8](https://doi.org/10.1007/s10509-014-2059-8)
- Brown, P. J., Dawson, K. S., Harris, D. W., et al. 2012, Astrophys. J., 749, 18, doi: [10.1088/0004-637X/749/1/18](https://doi.org/10.1088/0004-637X/749/1/18)
- Brown, P. J., et al. 2010, Astrophys. J., 721, 1608, doi: [10.1088/0004-637X/721/2/1608](https://doi.org/10.1088/0004-637X/721/2/1608)
- Brown, P. J., Hosseinzadeh, G., Jha, S. W., et al. 2019, ApJ, 877, 152, doi: [10.3847/1538-4357/ab1a3f](https://doi.org/10.3847/1538-4357/ab1a3f)
- Burns, C. R., Parent, E., Phillips, M. M., et al. 2018, ApJ, 869, 56, doi: [10.3847/1538-4357/aae51c](https://doi.org/10.3847/1538-4357/aae51c)
- Carnall, A. C. 2017, SpectRes: A Fast Spectral Resampling Tool in Python. <https://arxiv.org/abs/1705.05165>
- Chevalier, R. A., & Soderberg, A. M. 2010, ApJL, 711, L40, doi: [10.1088/2041-8205/711/1/L40](https://doi.org/10.1088/2041-8205/711/1/L40)
- Childress, M. J., et al. 2013, Astrophys. J., 770, 29, doi: [10.1088/0004-637X/770/1/29](https://doi.org/10.1088/0004-637X/770/1/29)
- . 2016, Publ. Astron. Soc. Austral., 33, e055, doi: [10.1017/pasa.2016.47](https://doi.org/10.1017/pasa.2016.47)
- Contreras, C., Phillips, M. M., Burns, C. R., et al. 2018, ApJ, 859, 24, doi: [10.3847/1538-4357/aabaf8](https://doi.org/10.3847/1538-4357/aabaf8)
- De, K., Kasliwal, M. M., Tzanidakis, A., et al. 2020, ApJ, 905, 58, doi: [10.3847/1538-4357/abb45c](https://doi.org/10.3847/1538-4357/abb45c)
- Dessart, L., Hillier, D. J., Li, C., & Woosley, S. 2012, Monthly Notices of the Royal Astronomical Society, 424, 2139, doi: [10.1111/j.1365-2966.2012.21374.x](https://doi.org/10.1111/j.1365-2966.2012.21374.x)
- Drout, M. R., Soderberg, A. M., Gal-Yam, A., et al. 2011, Astrophys. J., 741, 97, doi: [10.1088/0004-637X/741/2/97](https://doi.org/10.1088/0004-637X/741/2/97)
- Eldridge, J. J., Fraser, M., Smartt, S. J., Maund, J. R., & Crockett, R. M. 2013, Monthly Notices of the Royal Astronomical Society, 436, 774, doi: [10.1093/mnras/stt1612](https://doi.org/10.1093/mnras/stt1612)

- Filippenko, A. V. 1997, *Annual Review of Astronomy and Astrophysics*, 35, 309, doi: [10.1146/annurev.astro.35.1.309](https://doi.org/10.1146/annurev.astro.35.1.309)
- Firth, R. E., et al. 2015, *Mon. Not. Roy. Astron. Soc.*, 446, 3895, doi: [10.1093/mnras/stu2314](https://doi.org/10.1093/mnras/stu2314)
- Folatelli, G., Contreras, C., Phillips, M. M., et al. 2006, *The Astrophysical Journal*, 641, 1039, doi: [10.1086/500531](https://doi.org/10.1086/500531)
- Foley, R. J., Hoffmann, S. L., Macri, L. M., et al. 2020, *MNRAS*, 491, 5991, doi: [10.1093/mnras/stz3324](https://doi.org/10.1093/mnras/stz3324)
- Foley, R. J., et al. 2012, *Astrophys. J.*, 744, 38, doi: [10.1088/0004-637X/744/1/38](https://doi.org/10.1088/0004-637X/744/1/38)
- Fransson, C., et al. 2014, *Astrophys. J.*, 797, 118, doi: [10.1088/0004-637X/797/2/118](https://doi.org/10.1088/0004-637X/797/2/118)
- Fremling, C., Hall, X. J., Coughlin, M. W., et al. 2021, *SNIascore: Deep Learning Classification of Low-Resolution Supernova Spectra*. <https://arxiv.org/abs/2104.12980>
- Gal-Yam, A. 2017, *Observational and Physical Classification of Supernovae*, ed. A. W. Alsabti & P. Murdin (Cham: Springer International Publishing), 1–43, doi: [10.1007/978-3-319-20794-0_35-1](https://doi.org/10.1007/978-3-319-20794-0_35-1)
- Gal-Yam, A. 2019, *ARA&A*, 57, 305, doi: [10.1146/annurev-astro-081817-051819](https://doi.org/10.1146/annurev-astro-081817-051819)
- Gal-Yam, A., Kasliwal, M. M., Arcavi, I., et al. 2011, *ApJ*, 736, 159, doi: [10.1088/0004-637X/736/2/159](https://doi.org/10.1088/0004-637X/736/2/159)
- Gal-Yam, A., Bruch, R., Schulze, S., et al. 2021, *arXiv e-prints*, arXiv:2111.12435. <https://arxiv.org/abs/2111.12435>
- Ganeshalingam, M., Li, W., Filippenko, A. V., et al. 2010, *ApJS*, 190, 418, doi: [10.1088/0067-0049/190/2/418](https://doi.org/10.1088/0067-0049/190/2/418)
- Garavini, G., et al. 2007, *Astron. Astrophys.*, 471, 527, doi: [10.1051/0004-6361:20066971](https://doi.org/10.1051/0004-6361:20066971)
- Graham, M. J., Kulkarni, S. R., Bellm, E. C., et al. 2019, *PASP*, 131, 078001, doi: [10.1088/1538-3873/ab006c](https://doi.org/10.1088/1538-3873/ab006c)
- Graham, M. L., et al. 2017, *Mon. Not. Roy. Astron. Soc.*, 472, 3437, doi: [10.1093/mnras/stx2224](https://doi.org/10.1093/mnras/stx2224)
- Guillochon, J., Parrent, J., Kelley, L. Z., & Margutti, R. 2017, *ApJ*, 835, 64, doi: [10.3847/1538-4357/835/1/64](https://doi.org/10.3847/1538-4357/835/1/64)
- Hagberg, A. A., Schult, D. A., & Swart, P. J. 2008, in *Proceedings of the 7th Python in Science Conference*, ed. G. Varoquaux, T. Vaught, & J. Millman, Pasadena, CA USA, 11 – 15
- Hamuy, M., et al. 2002, *Astron. J.*, 124, 417, doi: [10.1086/340968](https://doi.org/10.1086/340968)
- Harris, C. R., Millman, K. J., van der Walt, S. J., et al. 2020, *Nature*, 585, 357, doi: [10.1038/s41586-020-2649-2](https://doi.org/10.1038/s41586-020-2649-2)
- Harutyunyan, A. H., et al. 2008, *Astron. Astrophys.*, 488, 383, doi: [10.1051/0004-6361:20078859](https://doi.org/10.1051/0004-6361:20078859)
- Ho, T. K. 1995, in *Proceedings of the Third International Conference on Document Analysis and Recognition (Volume 1) - Volume 1, ICDAR '95 (USA: IEEE Computer Society)*, 278
- Howell, D. A., Sullivan, M., Perrett, K., et al. 2005, *The Astrophysical Journal*, 634, 1190–1201, doi: [10.1086/497119](https://doi.org/10.1086/497119)
- Hunter, J. D. 2007, *Computing in Science & Engineering*, 9, 90, doi: [10.1109/MCSE.2007.55](https://doi.org/10.1109/MCSE.2007.55)
- Jenson, J. E., Prieto, J. L., Kochanek, C. S., et al. 2016, *Mon. Not. Roy. Astron. Soc.*, 456, 2622, doi: [10.1093/mnras/stv2795](https://doi.org/10.1093/mnras/stv2795)
- Kumar, B., Singh, A., Srivastav, S., Sahu, D. K., & Anupama, G. C. 2018, *Mon. Not. Roy. Astron. Soc.*, 473, 3776, doi: [10.1093/mnras/stx2498](https://doi.org/10.1093/mnras/stx2498)
- Magee, M. R., Maguire, K., Kotak, R., & Sim, S. A. 2021, *Monthly Notices of the Royal Astronomical Society*, 502, 3533–3553, doi: [10.1093/mnras/stab201](https://doi.org/10.1093/mnras/stab201)
- Matheson, T., Filippenko, A. V., Li, W., Leonard, D. C., & Shields, J. C. 2001, *Astron. J.*, 121, 1648, doi: [10.1086/319390](https://doi.org/10.1086/319390)
- Mauerhan, J. C., Smith, N., Filippenko, A. V., et al. 2013, *Monthly Notices of the Royal Astronomical Society*, 430, 1801–1810, doi: [10.1093/mnras/stt009](https://doi.org/10.1093/mnras/stt009)
- Maurer, I., Mazzali, P. A., Taubenberger, S., & Hachinger, S. 2010, *Monthly Notices of the Royal Astronomical Society*, 409, 1441, doi: [10.1111/j.1365-2966.2010.17186.x](https://doi.org/10.1111/j.1365-2966.2010.17186.x)
- Mazzali, P. A., Sauer, D. N., Pian, E., et al. 2017, *Monthly Notices of the Royal Astronomical Society*, 469, 2498, doi: [10.1093/mnras/stx992](https://doi.org/10.1093/mnras/stx992)
- Mazzali, P. A., et al. 2014, *Mon. Not. Roy. Astron. Soc.*, 439, 1959, doi: [10.1093/mnras/stu077](https://doi.org/10.1093/mnras/stu077)
- Minkowski, R. 1941, *PASP*, 53, 224, doi: [10.1086/125315](https://doi.org/10.1086/125315)
- Mirabal, N., Halpern, J. P., An, D., Thorstensen, J. R., & Terndrup, D. M. 2006, *The Astrophysical Journal*, 643, L99–L102, doi: [10.1086/505177](https://doi.org/10.1086/505177)
- Modjaz, M., Kirshner, R. P., & Challis, P. 2008, *Astrophys. J. Lett.*, 687, L9, doi: [10.1086/593135](https://doi.org/10.1086/593135)
- Modjaz, M., Liu, Y. Q., Bianco, F. B., & Graur, O. 2016, *ApJ*, 832, 108, doi: [10.3847/0004-637X/832/2/108](https://doi.org/10.3847/0004-637X/832/2/108)
- Modjaz, M., et al. 2014, *Astron. J.*, 147, 99, doi: [10.1088/0004-6256/147/5/99](https://doi.org/10.1088/0004-6256/147/5/99)
- Munari, U., Henden, A., Belligoli, R., et al. 2013, *New Astron.*, 20, 30, doi: [10.1016/j.newast.2012.09.003](https://doi.org/10.1016/j.newast.2012.09.003)
- Nakaoka, T., Kawabata, K. S., Maeda, K., et al. 2018, *ApJ*, 859, 78, doi: [10.3847/1538-4357/aabee7](https://doi.org/10.3847/1538-4357/aabee7)
- Nugent, P. E., et al. 2011, *Nature*, 480, 344, doi: [10.1038/nature10644](https://doi.org/10.1038/nature10644)
- Ostman, L., et al. 2011, *Astron. Astrophys.*, 526, A28, doi: [10.1051/0004-6361/201015704](https://doi.org/10.1051/0004-6361/201015704)

- Parrent, J. T., et al. 2012, *Astrophys. J. Lett.*, 752, L26, doi: [10.1088/2041-8205/752/2/L26](https://doi.org/10.1088/2041-8205/752/2/L26)
- Pastorello, A., et al. 2007, *Mon. Not. Roy. Astron. Soc.*, 376, 1301, doi: [10.1111/j.1365-2966.2007.11527.x](https://doi.org/10.1111/j.1365-2966.2007.11527.x)
- Pastorello, A., Mattila, S., Zampieri, L., et al. 2008, *MNRAS*, 389, 113, doi: [10.1111/j.1365-2966.2008.13602.x](https://doi.org/10.1111/j.1365-2966.2008.13602.x)
- Pastorello, A., Benetti, S., Brown, P. J., et al. 2015, *Monthly Notices of the Royal Astronomical Society*, 449, 1921, doi: [10.1093/mnras/stu2745](https://doi.org/10.1093/mnras/stu2745)
- Pedregosa, F., Varoquaux, G., Gramfort, A., et al. 2011, *Journal of Machine Learning Research*, 12, 2825
- Pereira, R., et al. 2013, *Astron. Astrophys.*, 554, A27, doi: [10.1051/0004-6361/201221008](https://doi.org/10.1051/0004-6361/201221008)
- Perets, H. B., Gal-Yam, A., Mazzali, P. A., et al. 2010, *Nature*, 465, 322, doi: [10.1038/nature09056](https://doi.org/10.1038/nature09056)
- Perlmutter, S., Aldering, G., Goldhaber, G., et al. 1999, *The Astrophysical Journal*, 517, 565, doi: [10.1086/307221](https://doi.org/10.1086/307221)
- Polin, A., Nugent, P., & Kasen, D. 2019, *The Astrophysical Journal*, 873, 84, doi: [10.3847/1538-4357/aafb6a](https://doi.org/10.3847/1538-4357/aafb6a)
- Prentice, S. J., & Mazzali, P. A. 2017, *Monthly Notices of the Royal Astronomical Society*, 469, 2672, doi: [10.1093/mnras/stx980](https://doi.org/10.1093/mnras/stx980)
- Prentice, S. J., Mazzali, P. A., Pian, E., et al. 2016, *MNRAS*, 458, 2973, doi: [10.1093/mnras/stw299](https://doi.org/10.1093/mnras/stw299)
- Prentice, S. J., Ashall, C., Mazzali, P. A., et al. 2018, *MNRAS*, 478, 4162, doi: [10.1093/mnras/sty1223](https://doi.org/10.1093/mnras/sty1223)
- Prentice, S. J., Ashall, C., James, P. A., et al. 2019, *MNRAS*, 485, 1559, doi: [10.1093/mnras/sty3399](https://doi.org/10.1093/mnras/sty3399)
- Qiu, Y., Li, W., Qiao, Q., & Hu, J. 1999, *AJ*, 117, 736, doi: [10.1086/300731](https://doi.org/10.1086/300731)
- Rabinak, I., & Waxman, E. 2011, *ApJ*, 728, 63, doi: [10.1088/0004-637X/728/1/63](https://doi.org/10.1088/0004-637X/728/1/63)
- Reis, I., Poznanski, D., Baron, D., Zasowski, G., & Shahaf, S. 2018, *Monthly Notices of the Royal Astronomical Society*, 476, 2117, doi: [10.1093/mnras/sty348](https://doi.org/10.1093/mnras/sty348)
- Riess, A. G., Filippenko, A. V., Challis, P., et al. 1998, *AJ*, 116, 1009, doi: [10.1086/300499](https://doi.org/10.1086/300499)
- Sako, M., Bassett, B., Becker, A. C., et al. 2018, *PASP*, 130, 064002, doi: [10.1088/1538-3873/aab4e0](https://doi.org/10.1088/1538-3873/aab4e0)
- Saselli, M., Hillebrandt, W., Aldering, G., et al. 2014, *Monthly Notices of the Royal Astronomical Society*, 447, 1247, doi: [10.1093/mnras/stu2416](https://doi.org/10.1093/mnras/stu2416)
- Saselli, M., Ishida, E. E. O., Vilalta, R., et al. 2016, *Monthly Notices of the Royal Astronomical Society*, 461, 2044, doi: [10.1093/mnras/stw1228](https://doi.org/10.1093/mnras/stw1228)
- Schlafly, E. F., & Finkbeiner, D. P. 2011, *ApJ*, 737, 103, doi: [10.1088/0004-637X/737/2/103](https://doi.org/10.1088/0004-637X/737/2/103)
- Shi, T., & Horvath, S. 2006, *Journal of Computational and Graphical Statistics*, 15, 118, doi: [10.1198/106186006X94072](https://doi.org/10.1198/106186006X94072)
- Shivvers, I., et al. 2017, *Publ. Astron. Soc. Pac.*, 129, 054201, doi: [10.1088/1538-3873/aa54a6](https://doi.org/10.1088/1538-3873/aa54a6)
- . 2019, *Mon. Not. Roy. Astron. Soc.*, 482, 1545, doi: [10.1093/mnras/sty2719](https://doi.org/10.1093/mnras/sty2719)
- Silverman, J. M., Ganeshalingam, M., & Filippenko, A. V. 2013, *Mon. Not. Roy. Astron. Soc.*, 430, 1030, doi: [10.1093/mnras/sts674](https://doi.org/10.1093/mnras/sts674)
- Silverman, J. M., et al. 2012, *Mon. Not. Roy. Astron. Soc.*, 425, 1789, doi: [10.1111/j.1365-2966.2012.21270.x](https://doi.org/10.1111/j.1365-2966.2012.21270.x)
- Simon, J. D., et al. 2007, *Astrophys. J. Lett.*, 671, L25, doi: [10.1086/524707](https://doi.org/10.1086/524707)
- Smith, N., Silverman, J. M., Filippenko, A. V., et al. 2012, *Astron. J.*, 143, 17, doi: [10.1088/0004-6256/143/1/17](https://doi.org/10.1088/0004-6256/143/1/17)
- Smitka, M. T., Brown, P. J., Kuin, P., & Suntzeff, N. B. 2016, *PASP*, 128, 034501, doi: [10.1088/1538-3873/128/961/034501](https://doi.org/10.1088/1538-3873/128/961/034501)
- Stahl, B. E., Zheng, W., de Jaeger, T., et al. 2019, *MNRAS*, 490, 3882, doi: [10.1093/mnras/stz2742](https://doi.org/10.1093/mnras/stz2742)
- . 2020, *MNRAS*, 492, 4325, doi: [10.1093/mnras/staa102](https://doi.org/10.1093/mnras/staa102)
- Sternberg, A., Gal-Yam, A., Simon, J. D., et al. 2011, *Science*, 333, 856, doi: [10.1126/science.1203836](https://doi.org/10.1126/science.1203836)
- Stritzinger, M., et al. 2002, *Astron. J.*, 124, 2100, doi: [10.1086/342544](https://doi.org/10.1086/342544)
- Stritzinger, M., Mazzali, P., Phillips, M. M., et al. 2009, *ApJ*, 696, 713, doi: [10.1088/0004-637X/696/1/713](https://doi.org/10.1088/0004-637X/696/1/713)
- Stritzinger, M. D., Anderson, J. P., Contreras, C., et al. 2018, *A&A*, 609, A134, doi: [10.1051/0004-6361/201730842](https://doi.org/10.1051/0004-6361/201730842)
- Stritzinger, M. D., et al. 2018, *Astron. Astrophys.*, 609, A135, doi: [10.1051/0004-6361/201730843](https://doi.org/10.1051/0004-6361/201730843)
- Sun, F., & Gal-Yam, A. 2017, *Quantitative Classification of Type I Supernovae Using Spectroscopic Features at Maximum Brightness*. <https://arxiv.org/abs/1707.02543>
- Terreran, G., Margutti, R., Bersier, D., et al. 2019, *ApJ*, 883, 147, doi: [10.3847/1538-4357/ab3e37](https://doi.org/10.3847/1538-4357/ab3e37)
- Valenti, S., et al. 2008, *Mon. Not. Roy. Astron. Soc.*, 383, 1485, doi: [10.1111/j.1365-2966.2007.12647.x](https://doi.org/10.1111/j.1365-2966.2007.12647.x)
- Valenti, S., Fraser, M., Benetti, S., et al. 2011, *Monthly Notices of the Royal Astronomical Society*, 416, 3138, doi: [10.1111/j.1365-2966.2011.19262.x](https://doi.org/10.1111/j.1365-2966.2011.19262.x)
- Valenti, S., Taubenberger, S., Pastorello, A., et al. 2012, *ApJL*, 749, L28, doi: [10.1088/2041-8205/749/2/L28](https://doi.org/10.1088/2041-8205/749/2/L28)
- Valenti, S., Howell, D. A., Stritzinger, M. D., et al. 2016, *MNRAS*, 459, 3939, doi: [10.1093/mnras/stw870](https://doi.org/10.1093/mnras/stw870)
- van der Maaten, L., & Hinton, G. 2008, *Journal of Machine Learning Research*, 9, 2579. <http://jmlr.org/papers/v9/vandermaaten08a.html>
- Vincenzi, M., Sullivan, M., Firth, R. E., et al. 2019, *Monthly Notices of the Royal Astronomical Society*, 489, 5802, doi: [10.1093/mnras/stz2448](https://doi.org/10.1093/mnras/stz2448)

- Vinkó, J., et al. 2018, *Publ. Astron. Soc. Pac.*, 130, 064101, doi: [10.1088/1538-3873/aab258](https://doi.org/10.1088/1538-3873/aab258)
- Wang, X., et al. 2009, *Astrophys. J.*, 697, 380, doi: [10.1088/0004-637X/697/1/380](https://doi.org/10.1088/0004-637X/697/1/380)
- Wes McKinney. 2010, in *Proceedings of the 9th Python in Science Conference*, ed. Stéfan van der Walt & Jarrod Millman, 56 – 61, doi: [10.25080/Majora-92bf1922-00a](https://doi.org/10.25080/Majora-92bf1922-00a)
- Williamson, M., Modjaz, M., & Bianco, F. B. 2019, *The Astrophysical Journal*, 880, L22, doi: [10.3847/2041-8213/ab2edb](https://doi.org/10.3847/2041-8213/ab2edb)
- Yamada, T., Kataoka, S., & Watanabe, K. 2010, *International Journal of Computer Mathematics*, 87, 3175, doi: [10.1080/00207160903329699](https://doi.org/10.1080/00207160903329699)
- Yamanaka, M., Maeda, K., Kawabata, M., et al. 2014, *ApJL*, 782, L35, doi: [10.1088/2041-8205/782/2/L35](https://doi.org/10.1088/2041-8205/782/2/L35)
- Yaron, O., & Gal-Yam, A. 2012, *Publications of the Astronomical Society of the Pacific*, 124, 668–681, doi: [10.1086/666656](https://doi.org/10.1086/666656)
- Yaron, O., et al. 2017, *Nature Phys.*, 13, 510, doi: [10.1038/nphys4025](https://doi.org/10.1038/nphys4025)
- Zhang, J., et al. 2018, *Astrophys. J.*, 863, 109, doi: [10.3847/1538-4357/aaceaf](https://doi.org/10.3847/1538-4357/aaceaf)
- Zhang, J.-J., Wang, X.-F., Bai, J.-M., et al. 2014, *AJ*, 148, 1, doi: [10.1088/0004-6256/148/1/1](https://doi.org/10.1088/0004-6256/148/1/1)
- Zhang, K., et al. 2016, *Astrophys. J.*, 820, 67, doi: [10.3847/0004-637X/820/1/67](https://doi.org/10.3847/0004-637X/820/1/67)
- Zhang, T., et al. 2012, *Astron. J.*, 144, 131, doi: [10.1088/0004-6256/144/5/131](https://doi.org/10.1088/0004-6256/144/5/131)